Third International Conference on CFD in the Minerals and Process Industries
CSIRO, Melbourne, Australia
10-12 December 2003

APPLICATION OF CFD IN VACUUM DEZINCING PROCESS

M.K. PATEL, C. BAILEY, G. DJAMBAZOV, J. SHRIMPTON and V. JALILI

[1]University of Greenwich, London, SE10 9LS, UK

ABSTRACT

Most lead bullion is refined by pyrometallurgical methods – this involves a series of processes that remove the antimony (softening) silver (Parkes process), zinc (vacuum dezincing) and if need be, bismuth (Betterton-Kroll process). The first step, softening, removes the antimony, arsenic and tin by air oxidation in a furnace or by the Harris process. Next, in the Parkes process, zinc is added to the melt to remove the silver and gold. Insoluble zinc, silver and gold compounds are skimmed of from the melt surface.

Excess zinc added during desilvering is removed from lead bullion using one of three methods:

- Vacuum dezincing;
- Chlorine dezincing; or
- Harris dezincing.

The present study concentrates on the Vacuum dezincing process for lead refining. The main aims of the research are to develop mathematical model(s), using Computational Fluid Dynamics (CFD) a Surface Averaged Model (SAM), to predict the process behaviour under various operating conditions, thus providing detailed information of the process - insight into its reaction to changes of key operating parameters. Finally, the model will be used to optimise the process in terms of initial feed concentration, temperature, vacuum height, cooling rate, etc.

NOMENCLATURE

A_f	time averaged area of blade	m/s
C_f	Drag coefficient	-
f	mole fraction	-
G	mass flux	kg/m^2
h	enthalpy	J/kg
h_c,h_s	thickness of steel lid, zinc crust	m
k	thermal conductivity	W/mK
M	mole mass	Kg/mol
n	number of blades	-
p_P	partial pressure	Pa
p^{vap}	equilibrium vapour pressure	Pa
Q	heat flux	W/m^2
R	gas constant	J/mol.K
r	radius	m
s	surface coefficient	-
T	absolute temperature	K
u	Velocity	m/s
λ	latent heat	J/kg
ρ	density	kg/m^3
μ	Kinematic Viscosity	m^2/s
ω	Rotational speed	Radians/s

Subscripts

B	bath surface
C	condenser surface

INTRODUCTION

Lead bullion is commonly refined by removing various impurities (e.g. copper, silver, bismuth, antimony, etc) sequentially. This in normally achieved by the addition of reagents which selectively react with the impurities and the resulting compounds removed by various means. To aid efficient mixing (ensure uniform reactions), batch mixing of materials via the aid of impellers is common practice in a number of industrial sectors. Excess zinc, added during the desilvering process can be removed by one of three methods: (1) **Vacuum dezincing** - During ***vacuum dezincing***, a vacuum is drawn on the agitated molten lead within a hemispherical vessel. Vaporized zinc condenses on the inner top surface of the vessel. The temperature at which zinc commences to vaporize lowers owing to heating under a vacuum. This enables vaporized zinc to be recovered in the form of high purity crystals without oxidation. The zinc crystals are recovered once the vessel lid is removed and the vacuum is broken. (2) **Chlorine dezincing** - In ***chlorine dezincing***, molten desilverised lead is reacted with chlorine gas, forming a surface layer of zinc chloride contaminated with small amounts of lead chloride. The layer is skimmed, treated with zinc for lead recovery. And finally (3) **Harris dezincing** - In ***Harris dezincing***, caustic soda saturated with lead oxide is mixed with molten lead in a reaction chamber, reducing lead oxide to lead and oxidizing zinc to zinc oxide. The zinc oxide reacts with the caustic to form sodium zincate. The contents of the reaction chamber are fed to a granulator and then reacted with hot water. Sodium zincate hydrolyses to zinc oxide and sodium hydroxide. Zinc oxide precipitates from solution, and is filtered, dried.

Of the three methods presented, the vacuum dezincing method is preferred, as it recovers zinc in the metallic state. This zinc metal, commonly known as vacuum zinc, is returned to the desilvering process.

Theoretical models of the vacuum process, for laminar flow in a launder, have been investigated (Davey, 1953). Nowadays refined models of the process can be built using CFD at various stages of the modelling, in order to obtain accurate results for the particular geometries and operating conditions of interest. Indeed, insight into the sensitivity of operating parameters can be investigated.

This paper presents the model(s) developed for the vacuum dezincing process together with insight into some of the key operating parameters for the process.

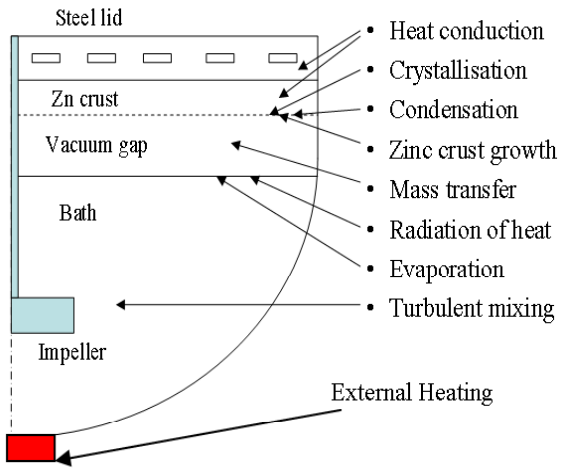

Figure 1: Schematic diagram of process physics

MODEL DESCRIPTION

Stages of the Dezincing Process

The zinc atoms leave the stirred liquid bath and are deposited across a vacuum gap in a solid crust growing on the inner surface of the lid of the kettle. The following stages of this transport process can be identified:

- transport of zinc through the liquid bath to its surface,

- evaporation of zinc,

- transport of zinc vapour through the vacuum gap,

- condensation and crystallisation of zinc.

The physics of evaporation, condensation and crust growth can be represented by a simpler Surface-Average Model without recourse to CFD. For the two transport stages, which involve convection and diffusion, CFD is an excellent simulation tool.

Surface-Average Model

Mass balance

The *evaporation* of a species from a multi-component system is governed by the Langmuir-Knudsen equation (Pehlke, 1979):

$$G_B = (p_B^{vap} - p_P)\, s_B f_B L_B \; ; \; L_B = \sqrt{\frac{M}{2\pi R T_B}} \qquad (1)$$

The *condensation* of zinc vapour onto the pure zinc crust (mole fraction = 1) can be described by a similar equation:

$$G_C = (p_P - p_C^{vap})\, s_C L_C \; ; \; L_C = \sqrt{\frac{M}{2\pi R T_C}} \qquad (2)$$

The *continuity* equation, in steady-state, requires that the evaporation and condensation mass fluxes are the same:

$$G_B = G_C \qquad (3)$$

and hence an expression for the average partial pressure of zinc vapour in the gap can be obtained:

$$p_P = \frac{p_B^{vap} s_B f_B L_B + p_C^{vap} s_C L_C}{s_B f_B L_B + s_C L_C} \qquad (4)$$

With the calculated partial pressure, the value of the vapour mass flux can be determined as per (1) and the growth of the crust thickness is easily represented by a temporal integral of this mass flux.

Heat balance

Given the thermal conductivities and the thicknesses of the zinc crust and the lid bottom respectively, the heat flux conducted through the lid can be expressed as a function of the boundary temperatures:

$$a_C = \frac{k_C}{h_C} \; ; \; a_S = \frac{k_S}{h_S} \; ; \; T_S = \frac{a_C T_C + a_S T_W}{a_C + a_S} \qquad (3)$$

$$Q_{LID} = a_C (T_C - T_S) \qquad (4)$$

where index $_S$ denotes the steel lid and T_S is at the interface between the lid bottom and the zinc crust; similarly, T_W is the temperature at the lower walls of the cooling water channels. On the other hand, the heat flux arising from condensation and crystallisation of the incoming mass flux can be calculated as:

$$Q_C = (\lambda_{evap} + \lambda_{fus})\, G_C \, . \qquad (5)$$

Conservation of heat in steady state requires the two heat fluxes to be equal:

$$Q_{LID} = Q_C \qquad (8)$$

and since both are functions of the crust surface temperature T_C , a *nonlinear equation* for it can be formulated and solved numerically.

Parameters

The average mole fraction of zinc on the surface of the bath f_B and the bath surface temperature T_B depend but are not equal to the corresponding values in the bulk of the bath. These dependences can be determined by CFD simulations (see below). Other important parameters are the cooling water temperature T_W, the initial concentration of zinc in the bath, the density of the zinc crust (which may be porous with non-uniform porosity) and the two surface activity coefficients s_B and s_C of the bath and crust respectively.

Bath Mixing Model

In some dezincing facilities the rate of the process is limited by diffusion dominated liquid-phase mass transfer (Warner, 1967). For the stirred kettle considered here this is unlikely to be the case, since turbulent mixing should be

supplying enough zinc to the surface of the bath. CFD simulations can provide quantitative data for the extent of mixing at a given speed of the shaft rotation. On that basis the *minimum* mixer speed can be determined for any particular geometry above which the bath can be assumed perfectly mixed. There is a possibility that, even at the minimum speed, splashes of bath can reach and contaminate the zinc crust. In this case the CFD results can be used to estimate how good or bad the mixing is at the lower 'safe' speed of rotation. Simulations of fluid flow and heat transfer within the bath have been carried out using PHYSICA V2.12.

Model Equations and Boundary Conditions

The CFD model equations used are summarised as follows

Mass Continuity Equation

$$\frac{d\rho}{dt} + div(\rho u) = 0 \qquad (9)$$

Momentum Equations

$$\frac{d(\rho\phi)}{dt} + div(\rho u\phi) = div(\mu grad\phi) + S_\phi \qquad (10)$$

where Φ = u, v or w, and the source term contains the pressure gradient

Energy Equation

$$\frac{d(\rho h)}{dt} + div(\rho uh) = div(kgradT) + S_h \qquad (11)$$

Turbulence is taken into account by using either a constant turbulent effective model or via the standard k-e turbulence model.

The blade is modelled using the source-sink approach for momentum sources (Pericleous and Patel, 1986, 1987). This approach uses blade element theory to calculate the momentum contributions arising from lift and drag components (Wallis, 1961), (Bertin and Smith, 1989). The advantage of such an approach is that the blades do not need to be meshed and modelled accurately, as it is assumed that the flow inside the impellers is averaged over the swept volume. Thus there is no direct simulation of the flow around the blades and furthermore, time-dependent interaction between the impellers and other internal obstructions (e.g. baffles) are all time-averaged. The advantage of such an approach is that it is fast and requires no experimental data – unlike the Direct Boundary Condition approach (Hamill and Hawkins, 1994). Indeed, the source-sink approach is thought to be the most suitable approach for many industrial applications which are concerned with what happens to the bulk of the material as opposed to flow behaviour close to the impellers. In recent years, the source-sink approach has been favoured over other approaches.

For the current study, a simple flat blade impeller is modelled. This type of blade is represented as a momentum source term in the tangential direction only, using the source term

$$S_{u_\theta} = \tfrac{1}{2}\rho\left[(\omega r) - u_\theta\right]^2 C_f n A_f \qquad (12)$$

where

C_f is the drag coefficient,
ωr is the local tangential velocity of the impeller,
n is the number of blades; and
A_f is the time averaged area swept by the blade.

This source term is added to the relevant direction momentum equation (10). Curved blade impellers and axial paddles can also be represented in a similar manner using momentum source terms in the tangential, radial and axial directions. For further details see Pericleous and Patel, 1986 and 1987.

Boundary Conditions

To complete the model definition, the following boundary conditions have been used for the mixing and temperature model:

(1) The shaft is represented with a blockage to the flow – all variables are initialised to zero within the shaft. Furthermore, the rotation of the shaft is imposed via the use of a wall-function shear term.

(2) At the vessel wall, a no-slip boundary condition is imposed - via the use of the log-law wall-function, which simulates the presence of a boundary layer.

(3) The liquid free surface is considered to be flat and frictionless. This could be further modified later to include a surface tracking model to predict the vortex depth. This would provide information relating to the rate of surface drawdown, an indicator of the time the material is exposed to the vacuum.

(4) At the bottom of the vessel a constant temperature boundary condition is imposed, to represent the heating element.

(5) At the bath surface a fixed flux boundary condition is applied to represent the cooling from the lid of the vessel.

Mesh and Convergence

Converged results for the mixing model were obtained within 25000 iterations with prescribed convergence criteria of 1e-6, for the continuity mass error. A typical mesh size used for the model was 40 x 60 cells in the radial and axial directions.

Gap Transport Model

There are two possible ways of looking at the flow of zinc vapour across the gap between the bath surface and the zinc crust at the lid. These are:

(1) Diffusion of zinc atoms through the residual gas (nitrogen; oxygen reacts and the oxides fall into the bath; Davey, 1953) and

(2) Resistance to the zinc vapour flow caused by the residual gas molecules which cannot be absorbed at the condenser/crust surface.

In the surface-average model presented above, the resistance to vapour flow in the vacuum gap height is ignored and thus the gap height does not appear in the model equations. This assumption is valid for high vacuums where molecular evaporation becomes dominant (Martin, 1956).

RESULTS

Bath Mixing

Natural Buoyancy Mixing

Initial results of the flow pattern within the vessel are obtained in the absence of a mixing device, here the mixing is aided via external heating of the melt - flow is wholly driven by buoyancy only. Figure 2a, presents the velocity distribution and the streamlines where as Figure 2b, presents the normalized temperature distribution at steady state. It is clearly evident that the flow from the base, at the centre, rises upwards and generates a single large recirculation region. This has an effect to wash the surface only near the central section of the surface. Furthermore, it is also evident that even at steady state, the bulk temperature is no way near uniform as the rate of heat loss is greater than the rate at which the bulk is being heated at. Clearly, this would not be the preferred route to heat and melt the bulk.

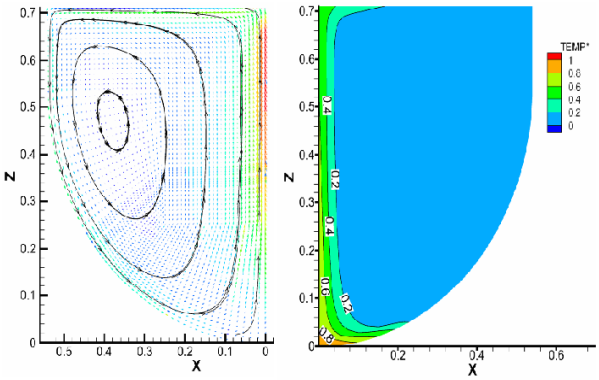

(a) (b)

Figure 2: (a) Velocity vectors and streamlines and (b) Normalized temperature profile

Forced Mixing

Initial results for the with-blade case have been obtained for velocity and normalized temperature distributions in the bath at 4 different impeller speeds, 150m 200, 250 and 300 rpm.

Figure 3(a-d) depict the velocity plots at the four speeds considered together with the streamlines. It is clear from the results that there is some surface washing occurring as the flow is drawn in from the centre. This is not an outcome of the blade (unlike an axial impeller) but is due to the high jet that emanates from the flat blade. It also clearly shows the existence of two distinct recirculation regions in the vessel, one above the blade and the other one below the blade. Indeed, at higher speeds material from the bottom half of the vessel is drawn into the upper half – evident from the closeness of the streamlines below the jet, near the wall.

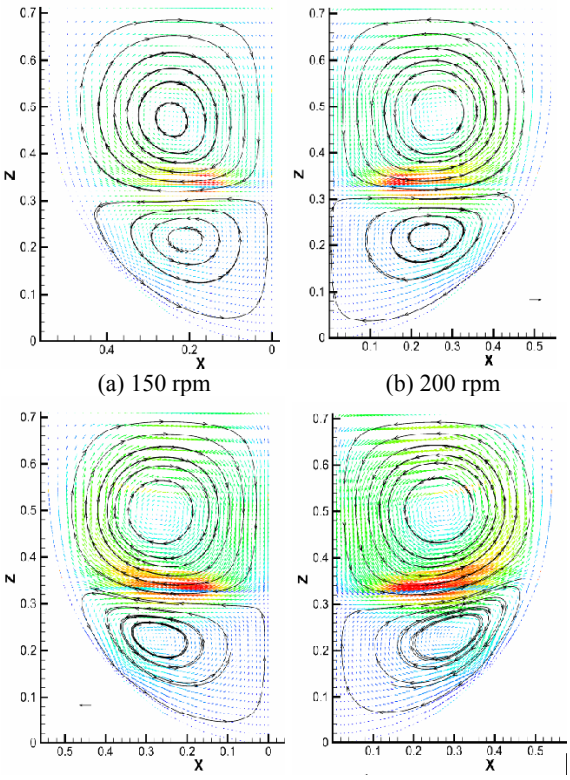

(a) 150 rpm (b) 200 rpm

(c) 250 rpm (d) 300 rpm

Figure 3: Velocity contours and streamlines

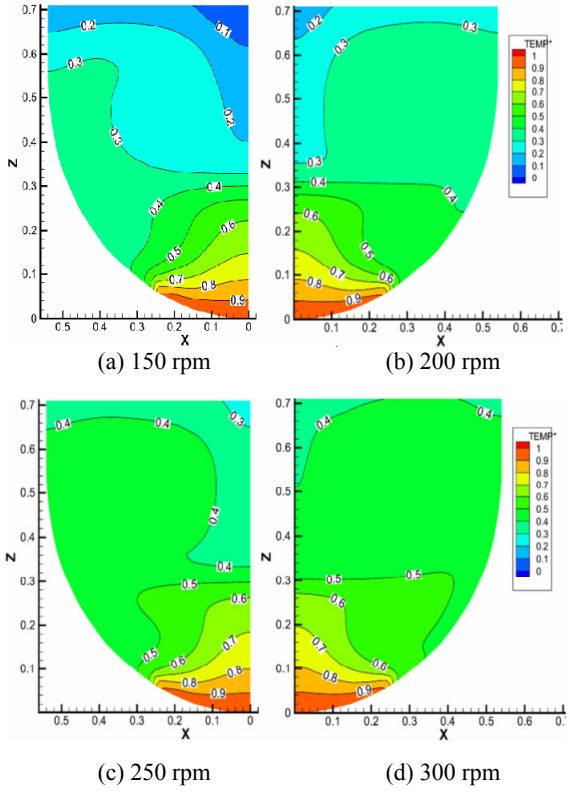

(a) 150 rpm (b) 200 rpm

(c) 250 rpm (d) 300 rpm

Figure 4: Temperature profiles

Results for the normalised temperature distribution for the four speeds are presented in Figure 4(a-d). It should be noted that the difference between the maximum and the minimum temperature in the above graphs is only a few degrees, so it is clearly evident that at low speeds, the surface remains cooler where as at higher speeds the material there is hotter thus the overall mixing is quite good.

Impeller Speed (rpm)	150	200	250	300
Ratio τ	0.9988	0.9991	0.9993	0.9994

Table 1: Mixing summary.

Defining a parameter, τ as the ratio of the surface-average temperature to the bulk volume-average temperature, then the variability of τ for each of the impeller speeds is tabulated in Table 1.

Bath temperature	T_B	600°C
Bath surface coefficient	s_B	0.4
Water temperature	T_W	50°C
Initial zinc concentration	wt%	20
Final zinc concentration	wt%	0.1
Process time	minutes	320
Steel layer thickness	h_S	5 mm
Maximum zinc crust height	h_C	21 cm
Steel thermal conductivity	k_S	47 W/m-K
Crust thermal conductivity	k_C	99 W/m-K
Latent heat of zinc evaporation	λ_{evap}	1784 kJ/kg
Latent heat of zinc fusion	λ_{fus}	111 kJ/kg
Condenser surface coefficient	s_C	0.5
Initial bath density	ρ_B	9620 kg/m^3
Zinc crust density	ρ_C	7100 kg/m^3
Radius of kettle	metres	1

Table 2: Process Parameters.

Process Rate

Various scenarios were considered to evaluate the sensitivity of controllable parameters of the process. These included:

- Vacuum Gap Height
- Zinc Crystal Porosity
- Initial Zinc concentration in the Bulk
- Temperature of the Bulk
- Heat Transfer at the Lid
- Mixing Rate
- Activity Coefficients at the Bath Surface

Sample results, using the set of parameters presented in Table 2, together with the surface-average model have been used to obtain results presented in Figures 5-7.

The time step for the fully-explicit temporal integration was 10 s, and the solution method for the nonlinear algebraic equation about the crust front temperature T_C was via a binary search. The molar mass of zinc is M = 0.06538 kg/mol, the gas constant is R = 8.3145 J/mol-K and the equilibrium vapour pressure of zinc was calculated from the formula (Alcock, 2001):

$$\log\ p^{vap}\ (\text{atm}) = 5.378\ -\ 6286\ /\ T \qquad (12)$$

Figure 5 presents the evolution of the space-averaged process variables using process parameters presented in Table 2.

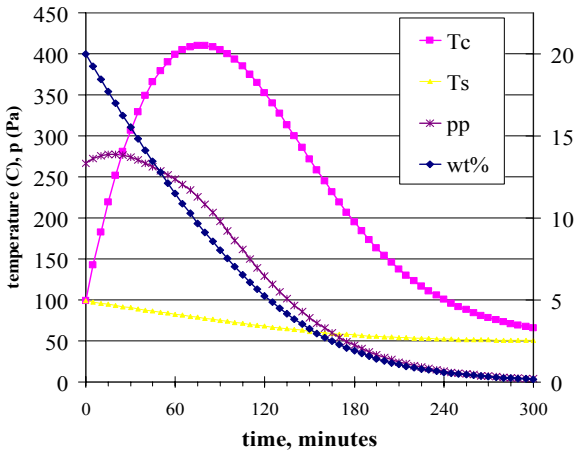

Figure 5: Evolution of space-averaged process variables.
Tc - crust temperature; **Ts** - Steel lid temperature;
pp - Partial Pressure; **Wt%** - Zn conc. bath

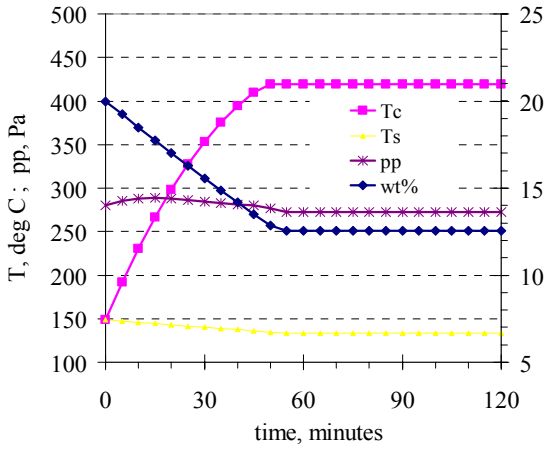

Figure 6: Evolution of space-averaged process variables, Water temperature = 100°C.
Tc - crust temperature; **Ts** - Steel lid temperature;
pp - Partial Pressure; **Wt% -** Zn conc. bath

It can be seen that the peak of the surface temperature, T_C, is too close to the melting point of zinc 420°C. This means that the rate limiting step of the process at high initial zinc concentrations is the heat transfer through the fast growing zinc crust. This means that in the worst case scenario, the process could get to a steady-state solution where the rate of crystallisation is equal to the rate of melting at the collector surface – in which case the bulk melt would no longer be depleting in zinc concentration.

Figure 6 presents the evolution of the space-averaged process variables using process parameters presented in Table 2, except now the water temperature is elevated to 100°C. It is clear, from Figure 6, that this increase in temperature is undesirable as the process reaches pseudo

steady-state at around 50 minutes, after which there is no further decrease of the bulk zinc concentration.

Indeed, the obvious action to take, when the zinc crust is beyond a calculated thickness, is to undertake a "lid-clean". For the given operation conditions, this would be necessary at around 50 minutes. Once the process is restarted, the bath concentration of zinc proceeds to reduce relatively quickly to a desired level.

Figure 7, presents the same scenario as that of Figure 6, except in this case the lid has been cleaned at 50 minutes – this corresponds to the sharp drop in the value of Tc. However, once the lid has been replaced, and the process allowed to continue, it is clear that the zinc concentration in the bulk drops down to acceptable levels and no longer plateaus out to an undesirable high concentration.

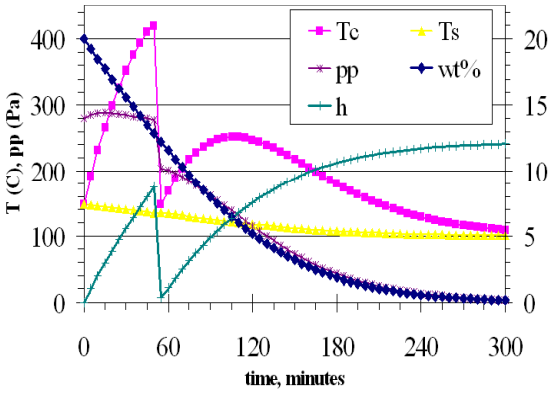

Figure 7: Evolution of space-averaged process variables, Water temperature = 100°C – with crust removal at 50 minutes.
Tc - crust temperature; **Ts** - Steel lid temperature;
pp - Partial Pressure; **Wt% -** Zn conc. Bath;
h – thickness of zinc crust

Similarly, one can vary the key parameter of importance to the process and arrive at the optimum rate at which the zinc is extracted - depending on the desired mode of operation of the process.

Finally, since the simulations are quick, it is possible to provide the operator with precise information depending on the zinc concentration within the bulk at the start-up of a new batch.

CONCLUSION AND FURTHER WORK

In conclusion, it has been demonstrated that a model that described the vacuum dezincing process has been formulated with the aid of a Surface Average Model, based on 2-dimensions Computational Fluid Dynamics simulations and a 1-dimensional thermal model of the behaviour of the vacuum dezincing process. The model has been tested for it robustness. It is demonstrated that the model is dependent on a number of key parameters, some of the sensitivity analysis demonstrating the importance of "control" necessary to achieve "good" performance.

A number of tasks remain to ensure that the model is integrated within the production floor. These are:

- Gather "quality" experimental data from a prototype small scale process
- Validate the model
- Optimise the model for the prototype process
- Extend the model for to large scale process
- Validate the model for large scale process.

The models also need to be integrated into an engineering framework for industrial use. These are the next challenging phases that are currently being undertaken.

REFERENCES

ALCOCK, C.B., (2001), "Thermochemical processes: principles and models", Butterworth-Heinemann.

BERTIN, J.J. and SMITH, M.J., (1989), Aerodynamics for Engineers (Prentice-Hall Inc., Englewood Cliffs, New Jersey, USA)

DAVEY, T.R.A., (1953), "Vacuum dezincing of desilverised lead bullion", J. Metals, Aug., 991-997.

HAMILL, I.S., and HAWKINS, I.P., (1994), The application of CFDS-FLOW3D to single- and multi-phase flows in mixing vessels, AIChE Annual meeting, Session 186, Paper Number 186g

MARTIN, A.J., (1956), "Vacuum distillation of metals", Metal Industry, June, 473-476.

PEHLKE, R.D., (1979), "Unit Processes of Extractive Metallurgy", Elsevier Publishing Co.

PERICLEOUS, K.A., and PATEL, M.K., (1986), "The modelling of tangential and axial agitators in chemical reactors", PCH Physiochemical Hydrodynamics, Vol 8, 105-123

PERICLEOUS, K.A., and PATEL, M.K., (1987), The source-sink approach in the modelling of stirred reactors, PCH Physiochemical Hydrodynamics, Vol 9, 279-297

PHYSICA Multi-Physics Modelling Code. University of Greenwich, Old Royal Naval College, 30 Park row, Greenwich, London SE10 9LS. Physica@gre.ac.uk

WALLIS, R.A., (1961), Axial Flow Fan: Design and Practice (London: Newnes, London)

WARNER, N.A., (1967), "Kinetics of continuous vacuum dezincing of lead", Advances in Extractive Metallurgy, IMM, London, 317-332.

ACKNOWLEDGEMENT

The authors would like to acknowledge the collaboration and contributions of Prof. Derek Fray and Dr Tony Cox (University of Cambridge), Mr Ivan Forsdick and Mr Peter Moor (Britannia Refined Metals - UK) and the financial support provided by the Engineering and Physical Sciences Research Council (EPSRC, UK).